Zero-shell diffusion MRI:
Accessing tissue microstructure without oversampling fiber orientations

Santiago Coelho
Els Fieremans
Dmitry S. Novikov

Center for Biomedical Imaging,
Department of Radiology,
NYU Grossman School of Medicine

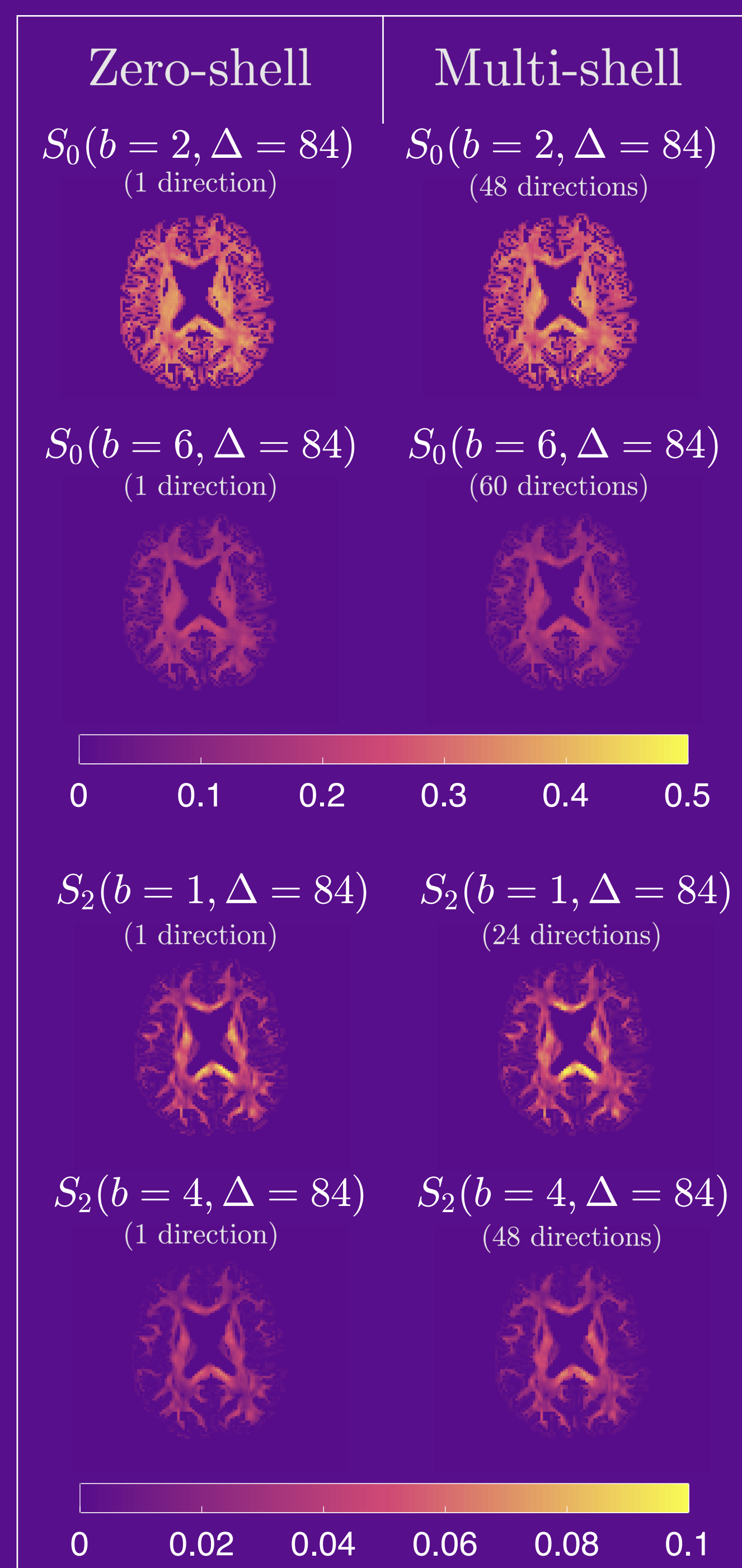| Zero-shell	Multi-shell
$S_0(b=2, \Delta=84)$ (1 direction)	$S_0(b=2, \Delta=84)$ (48 directions)
$S_0(b=6, \Delta=84)$ (1 direction)	$S_0(b=6, \Delta=84)$ (60 directions)
$S_2(b=1, \Delta=84)$ (1 direction)	$S_2(b=1, \Delta=84)$ (24 directions)
$S_2(b=4, \Delta=84)$ (1 direction)	$S_2(b=4, \Delta=84)$ (48 directions)

Figure 4. Comparison of rotational invariants ($\ell=0,2$) computed from the zero-shell and multi-shell acquisitions.

INTRODUCTION

In biophysical modeling we interested in microstructure parameters of fiber bundles[1-13,16]:

- Compartment fractions, diffusivities, relaxation rates, exchange, structural disorder, …

To measure them we can jointly sample multiple: diffusion weightings, tensor shapes, diffusion times, echo times, …

- Most of scan time is spent on oversampling the fODF of these bundles
- **This disproportionate oversampling of directions to factor out fODF[8-11] is a giant scan-time sink and an unresolved problem so far**

We want to measure multiple combinations of experimental parameters, spending a single gradient direction per combination, allowing denser exploration of the diffusion acquisition space.

- We use svd to recover signal rotational invariants for all (b, Δ), allowing extensive modeling/analysis

Figure 1. Zero-shell dMRI acquisition protocol.

THEORY

In many tissues, e.g. white and gray matter, the diffusion signal can be modeled as a convolution[1-8,12,13]:

$$S(b, \Delta, \hat{\mathbf{g}} \mid x, p_{\ell m}) = \int_{\mathbb{S}^2} d\hat{\mathbf{n}}\, \mathcal{K}(b, \Delta, \hat{\mathbf{g}} \cdot \hat{\mathbf{n}} \mid x)\, \mathcal{P}(\hat{\mathbf{n}} \mid p_{\ell m}) = \sum_{n'} S_{n'}\, U_{n'}(b, \Delta, \hat{\mathbf{g}})\, V_{n'}(x, p_{\ell m}) \quad (1)$$

- Without assumptions on the kernel $\mathcal{K}(b, \Delta, \ldots \mid x)$, akin to [14] we can write

$$S(b, \Delta, \hat{\mathbf{g}} \mid x, p_{\ell m}) = \sum_{\ell m} S_{\ell m}(b, \Delta) Y_{\ell m}(\hat{\mathbf{g}}) = \sum_{\ell m} K_\ell(b, \Delta \mid x) p_{\ell m} Y_{\ell m}(\hat{\mathbf{g}}) \quad (2)$$

$$\mathcal{K}_\ell(b, \Delta \mid x) \simeq \sum_{n=1}^{N_\ell} s_n^{(\ell)} u_n^{(\ell)}(b, \Delta) v_n^{(\ell)}(x) \quad (3)$$

Substituting (3) in (1), where U depends on protocol and V on tissue:

$$S(b, \Delta, \hat{\mathbf{g}} \mid x, p_{\ell,m}) = \sum_{\ell m n} s_n^{(\ell)} u_n^{(\ell)}(b, \Delta) Y_{\ell m}(\hat{\mathbf{g}}) v_n^{(\ell)}(x) p_{\ell m} = \sum_{\ell m n} \alpha_{\ell m n} \gamma_{\ell m n} \quad (4)$$

- The spherical convolution allows us to assign 'quantum numbers' ℓ, m, n, to the columns of $U_{n'}$
- This results in $2\ell+1$-degenerate singular values or "*multiplets*" (Fig. 2)

Figure 2. Singular values of a large set of DWI from simulations and brain data. Degenerate singular values on each degree l of the ODF are observed exactly on simulated data and with some repulsion in the noisy data.

Without assumptions on the kernel's functional form, we can reconstruct all rotational invariants:

$$S_\ell(b, \Delta \mid x, p_\ell) = \frac{1}{2\ell+1} \sum_n \tilde{\alpha}_{\ell n} \tilde{\gamma}_{\ell n} \quad (5)$$

- Correct signs must be estimated:

$$\alpha_{n\ell} = ||\alpha_{n\ell m}||^{(m)} = \sqrt{\sum_m \alpha_{n\ell m}^2} = \sqrt{\frac{2\ell+1}{4\pi}} |u_n^{(\ell)}(b, \Delta)|, \quad \tilde{\alpha}_{n\ell} = \alpha_{n\ell} \times \text{sign}(u_n^{(\ell)}(b, \Delta))$$

$$\gamma_{n\ell} = ||\gamma_{n\ell m}||^{(m)} = \sqrt{\sum_m \gamma_{n\ell m}^2} = \sqrt{4\pi(2\ell+1)}\, p_\ell\, |v_n^{(\ell)}(x)|, \quad \tilde{\gamma}_{n\ell} = \gamma_{n\ell} \times \text{sign}(v_n^{(\ell)}(x))$$

EXPERIMENTS

A healthy 25yo male was scanned on a 3T-system (Siemens Prisma) w/32ch head coil at: 2x2x2mm³, TE=120ms, TR=5s, BW=2272Hz/Px, R=2, PF=6/8, t_{acq}=55 min. A monopolar PGSE sequence was used to acquire 550 uniform directions, each w/ unique (b, Δ) (Fig. 1).

RESULTS

SVD of simulated voxels according to the Standard Model, as well as measured human white and gray matter, are shown in Fig. 2.

- Projecting $U_{n'}(b, \Delta, \hat{\mathbf{g}})$ on spherical harmonics enables robust $\ell, m, n,$ assignment and subsequent sign estimation for $u_n^{(\ell)}$ and $v_n^{(\ell)}$

Rotational invariants reconstructed with Eq. (5) for WM/GM regions are shown in Fig. 3.

- Additional validation shells show accurate predictions of rotational invariants (Fig. 4)

We can use rotational invariants to compute DTI/DKI and study their time dependence, in agreement with[15], or to estimate any given biophysical model such as the Standard Model Imaging (SMI)[16] in WM or Neurite Exchange Imaging (NEXI)[12] for GM (Fig. 6).
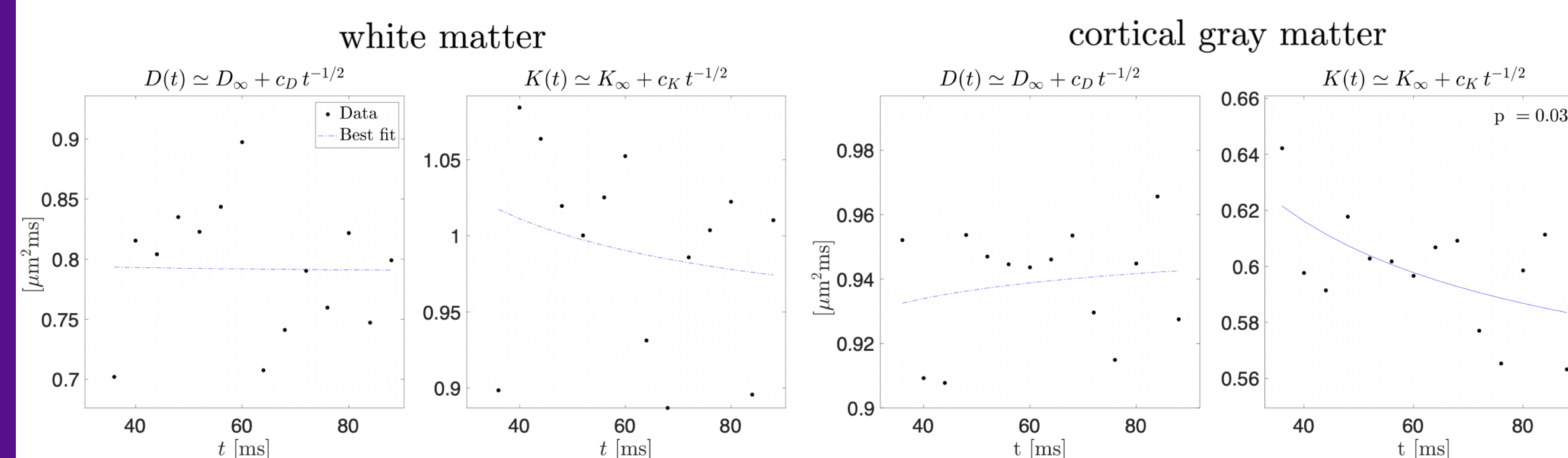

Figure 3. Rotational invariants reconstructed for each combination of (b, Δ). Note that only 1 direction was sampled for each pair.

Figure 5. Diffusion and kurtosis time dependence for white and gray matter. Only mean kurtosis is significant[15].

Figure 6. Model parameter maps computed from rotational invariants for white and gray matter.

DISCUSSION AND CONCLUSION

We measured dMRI signals at 550 distinct (b, Δ) combinations and computed rotational invariants for all. **No assumptions were made on the functional form of the tissue response function**, only the convolution with fODF. This method provides **massive time savings for multi-dimensional dMRI**.

- The number of distinct $s_n^{(\ell)}$ above the noise floor provides an upper limit to the number of degrees of freedom necessary for modeling the kernel
- We show how one can measure multiple inequivalent combinations of experimental parameters – e.g., b and Δ – while spending only a single gradient direction per unique combination (b, Δ). This is extendable for B-tensor shapes, TE, etc

REFERENCES

[1] D. S. Novikov, et al., NMR Biomed., e3998, 2019.
[2] C. D. Kroenke, et al., Magn. Reson. Med., 52, 5, 1052–1059, 2004.
[3] Y. Assaf, et al., Magn. Reson. Med., 52, 965–978, 2004.
[4] S. N. Jespersen, et al., NeuroImage, 34, 1473–1486, 2007.
[5] E. Fieremans, et al., Proc ISMRM, 2012.
[6] H. Zhang, et al., NeuroImage, 61, 1000–1016, 2012.
[7] J. H. Jensen, et al., NeuroImage, 124, 824–833, 2016.
[8] M. Reisert, et al., NeuroImage, 147, 964-975, 2017.
[9] S. Jespersen, et al., NMR Biomed, 26, 1647-1662, 2013.
[10] E. Kaden, et al., NeuroImage, 139, 346-359, 2016.
[11] D. S. Novikov, et al., NeuroImage, 174, 518 – 538, 2018.
[12] I. Jelescu, et al., NeuroImage, 256, 119277, 2022.
[13] J. Olesen, et al., NeuroImage, 251, 118976, 2022.
[14] D. Christiaens, et al., IEEE TMI 38, 3, 2019.
[15] H-H. Lee, et al. NeuroImage, 222,117054, 2022.
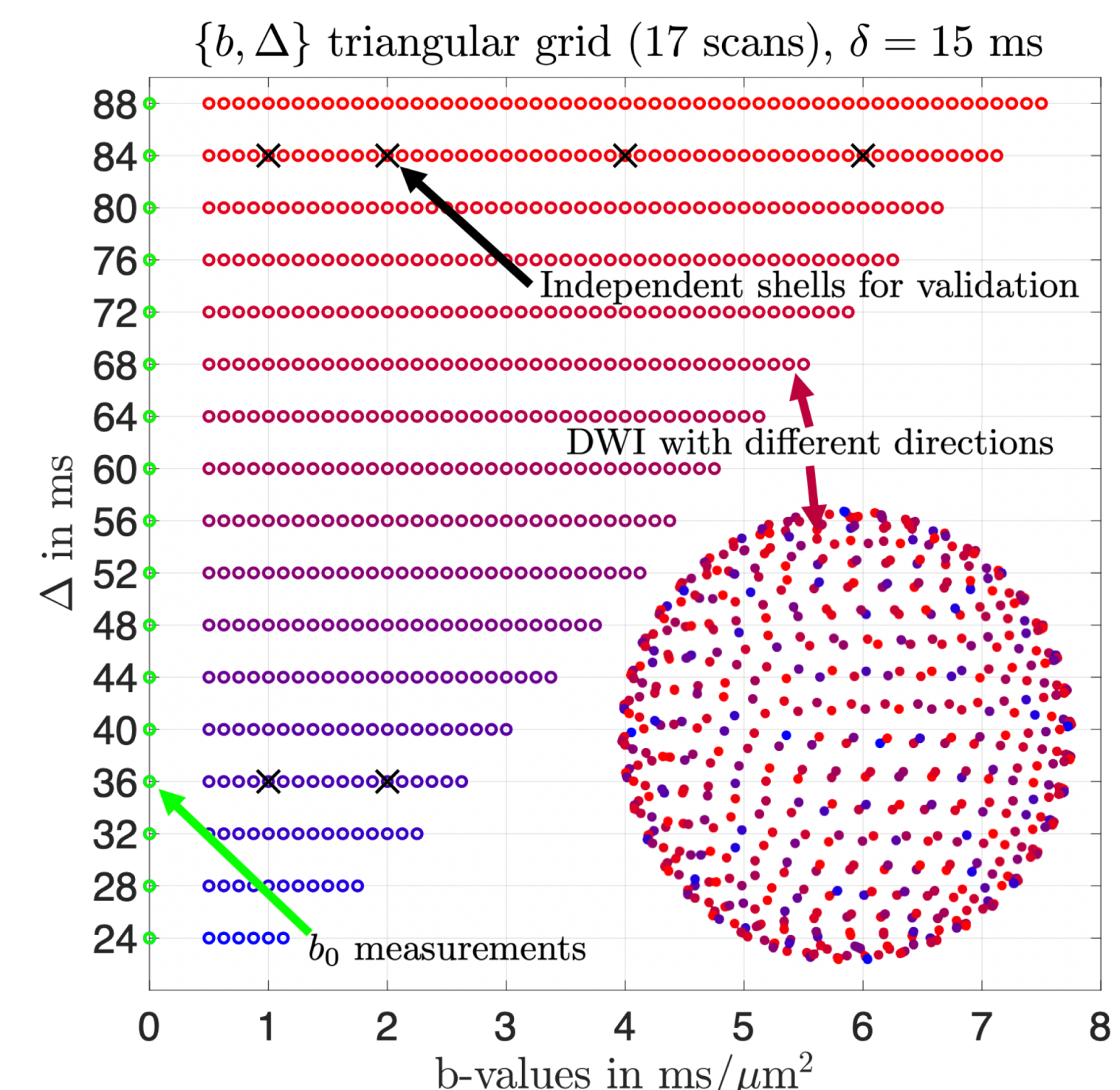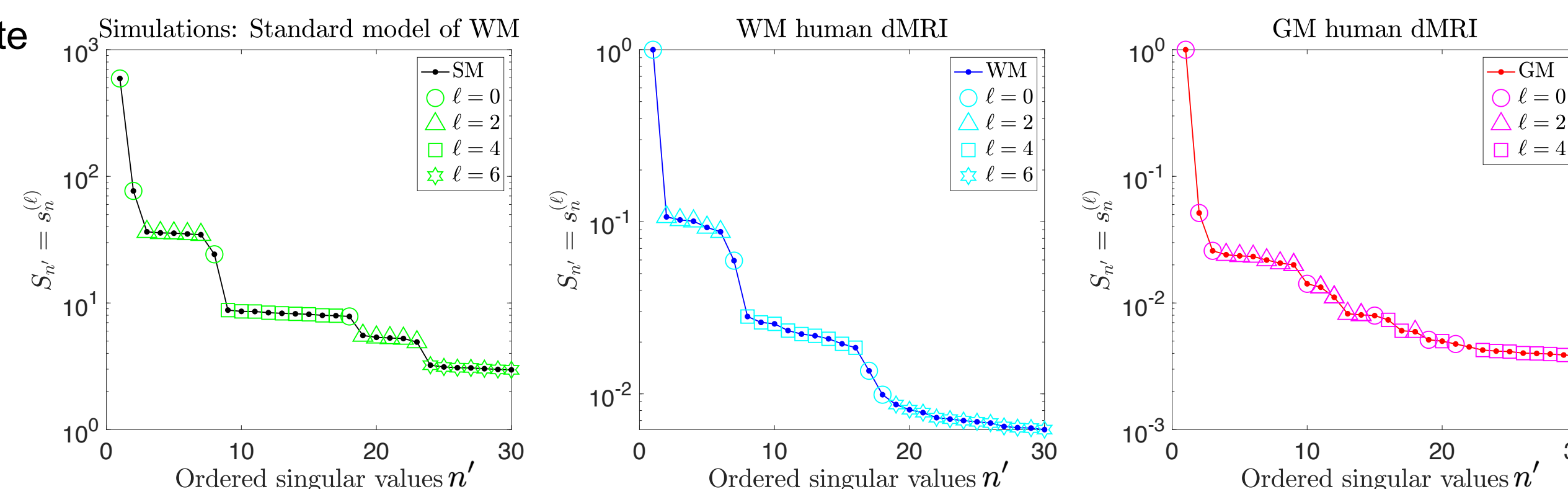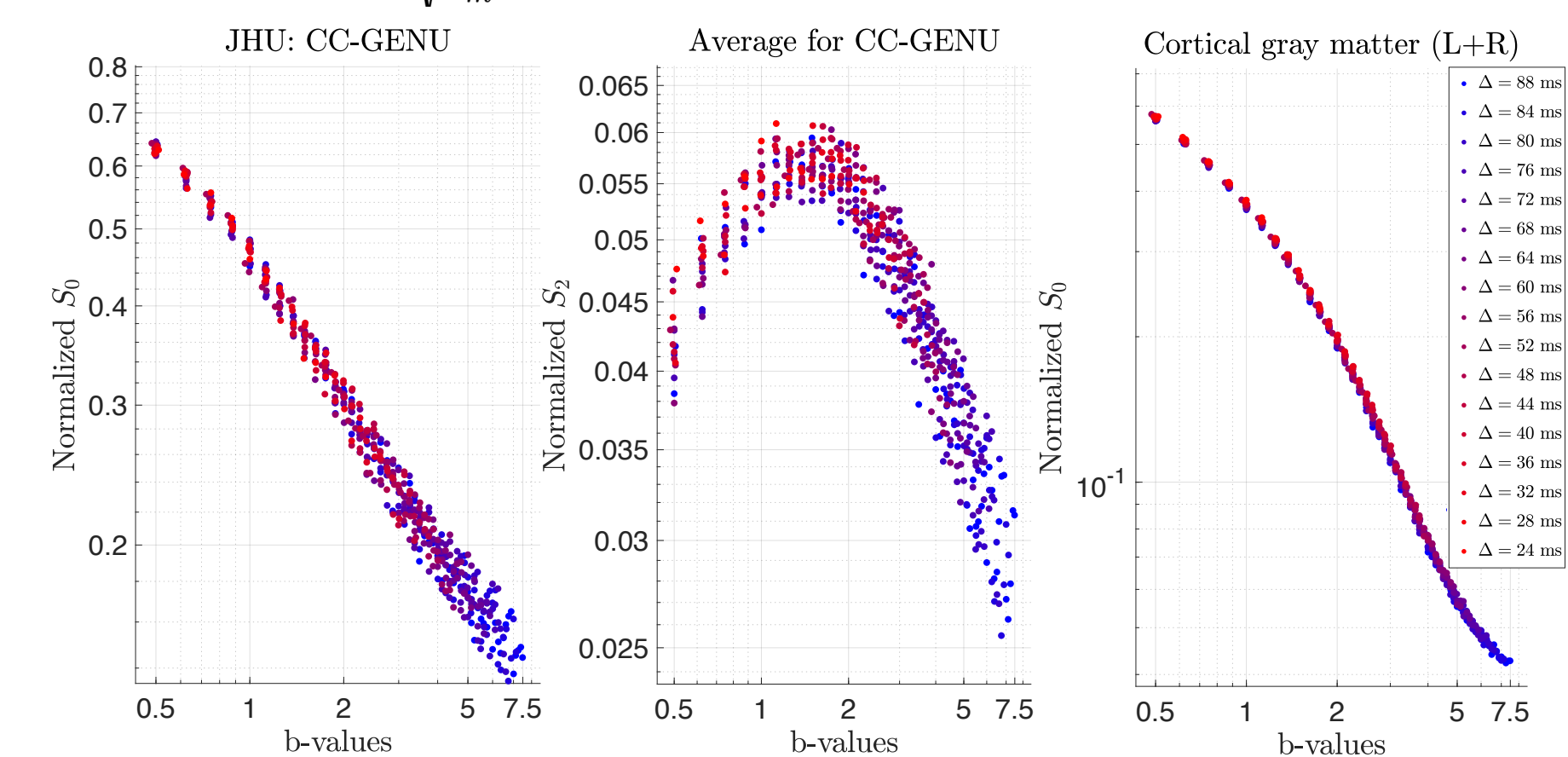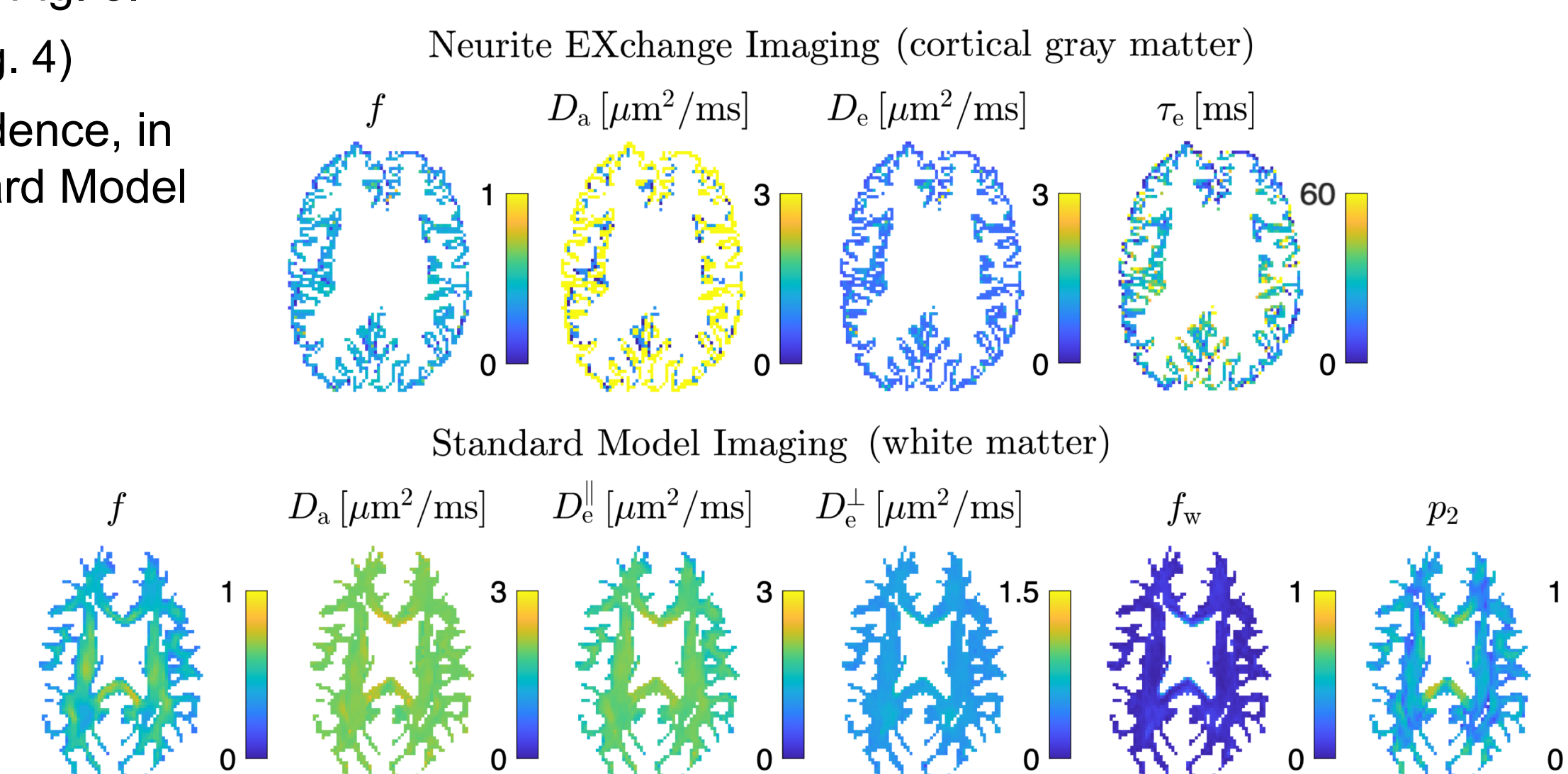[16] S. Coelho, et al., NeuroImage, 257, 119290, 2022.

CAI²R Center for Advanced Imaging Innovation and Research

NYU Grossman School of Medicine

Center for Biomedical Imaging

@santicoelho   Santiago.Coelho@nyulangone.org